

Gate-Dependent Electronic Raman Scattering in Graphene

E. Riccardi,^{*} M.-A. Méasson, M. Cazayous, A. Sacuto, and Y. Gallais[†]

*Laboratoire Matériaux et Phénomènes Quantiques (UMR 7162 CNRS), Université Paris Diderot-Paris 7,
Bâtiment Condorcet, 75205 Paris Cedex 13, France*

(Received 7 September 2015; published 11 February 2016)

We report the direct observation of polarization resolved electronic Raman scattering in a gated monolayer graphene device. The evolution of the electronic Raman scattering spectra with gate voltage and its polarization dependence are in full agreement with theoretical expectations for nonresonant Raman processes involving interband electron-hole excitations across the Dirac cone. We further show that the spectral dependence of the electronic Raman scattering signal can be simply described by the dynamical polarizability of graphene in the long wavelength limit. The possibility to directly observe Dirac fermion excitations in graphene opens the way to promising Raman investigations of electronic properties of graphene and other 2D crystals.

DOI: 10.1103/PhysRevLett.116.066805

Graphene is a unique system consisting of a single layer of honeycomb carbon lattice. The exceptional physical properties of graphene are determined by its peculiar electronic structure near the Dirac point, where the linear dispersion allows us to describe the graphene electrons as massless relativistic particles [1–3]. Optical spectroscopies are an attractive alternative to electrical transport for probing electronic excitations and excited-state properties of graphene [4,5], and both infrared (IR) and THz spectroscopies have been applied successfully to probe carrier dynamics near the Dirac point [6–12]. Some of these studies were performed on gated graphene devices, allowing a fine tuning of the Fermi level in order to study both intraband (Drude) excitations in the THz regime and interband excitations on the midinfrared regime. Midinfrared measurements were also extended at high magnetic field where Landau level transitions could be observed [13–15]. However, because of inherent limitations due to the large photon wavelength in the IR, most of these studies have been limited to relatively large area samples such as CVD grown graphene, which are still limited in terms of mobility, or graphene on SiC, where the carrier density cannot be tuned by a gate voltage. This has somewhat hampered the study of electronic interaction effects by spectroscopy as the extracted scattering rates are probably dominated by disorder effects.

Raman inelastic light scattering is, in principle, an attractive alternative to the above spectroscopies because it is a low frequency spectroscopy (from the mid-IR down to the THz regime) and due to the fact that it uses visible photons, it has a submicron spatial resolution, therefore allowing the study of a wider array of graphene devices including the cleanest ones. Raman spectroscopy holds indeed a privileged position in the study and characterization of graphitic materials. Up to now, its use in graphene has been almost exclusively limited to the study of optical

phonons, whose properties as a function of the number of layers, chemical doping, gate voltage, and stress have been extensively investigated [16,17]. In particular, studies on gated graphene devices were able to extract information on the electronic properties of graphene both at zero [18–20] and finite [21–23] magnetic field via electron-phonon coupling effects which strongly renormalize the *G*-band optical phonon self-energy. More recently, the observation of electronic Raman scattering by inter-Landau level excitations was reported at high-magnetic fields [24–26]. Despite these advances, direct observation of electronic Raman scattering (ERS) at zero-magnetic field has remained up to now rather elusive. A recent work has shown that the background of the Raman spectra of graphene is strongly dependent on the nature of the substrate, making it difficult to isolate the ERS contribution [27]. Contrary to the case of high magnetic field where sharply-defined Landau levels develop in the electronic structures, the expected ERS spectrum at zero field is almost featureless, making it difficult to be distinguished from the background signal. In addition, contrary to semiconductor heterostructures with a direct optical band gap, and also to carbon nanotubes [28], the ERS process in graphene is, except for very high electron or hole dopings, nonresonant. It has thus remained unclear whether the ERS cross section for a 1 atom thick graphene layer is large enough to be detected and extracted from the background signal inherent to any Raman experiment.

In this Letter we report the unambiguous observation of the ERS signal at zero magnetic field in a gated monolayer graphene device. The evolution of the ERS spectra and its polarization dependence are in full agreement with theoretical expectations of the evolution of interband electron-hole excitations upon varying gate voltage [29,30]. The observed ERS continuum is weak, about 100 times weaker than the 2D optical phonon band. It displays a suppression due to Pauli blocking at a threshold close to the frequency

$\omega = 2E_F$, which shifts under the application of a gate voltage. Polarization resolved measurements indicate that the ERS signal has A_{2g} symmetry as expected for vertical interband transitions across the Dirac cone in graphene [29]. The extracted evolution of the Fermi energy with the gate voltage agrees very well with the estimated capacitance of the device and the Fermi velocity of graphene. The evolution of the ERS continuum is also entirely consistent with the observed broadening of the G -band optical phonon, providing a unified picture of the two processes, which are both controlled by the electronic polarizability of graphene [31].

The graphene-based device studied was produced by exfoliation of natural graphite. Electrical contacts were first produced using e -beam lithography and Pd deposition on an oxidized Si wafer $\text{SiO}_2 \sim 280$ nm). The preidentified graphene flake was then positioned using a dry transfer technique [32] on the top of the Si/SiO₂ device. The resulting structure is relatively standard and allows us to apply a gate voltage between the graphene sample and the doped Si substrate that acts as a back gate.

Polarization resolved Raman scattering measurements were performed using a home-built micro-Raman setup in a backscattering configuration equipped with a motorized xyz stage with submicron spatial resolution. The $\lambda = 532$ nm (2.33 eV) excitation line of a Diode Pumped Solid State (DPSS) Laser was focused onto the sample using a long working distance $100\times$ objective lens. The laser spot was $\leq 1 \mu\text{m}$ and all measurements were performed with an incident laser power less than 1 mW to avoid any significant heating effects. All measurements were performed in the vacuum chamber ($P < 10^{-5}$ mbar) of a low temperature optical cryostat. The lowest cold finger temperature achieved was 30 K. The excitation beam and the collected signal were linearly polarized in order to identify the symmetry of the Raman active excitations. Using the irreducible representations of the D_{6h} point group, the A_{1g} and E_{2g} symmetries were probed in parallel polarizations geometry and the A_{2g} and E_{2g} in the cross-polarizations geometry [33]. Integration times of several minutes were typically used for each spectra. The device and the optical setup are illustrated in Fig. 1(a).

Figure 1(b) shows polarization resolved spectra recorded at 0 and -40 V, in the $0 - 6000 \text{ cm}^{-1}$ range and at $T = 30$ K. The Raman signal below 1100 cm^{-1} is dominated by the contribution of the doped Si layer of the substrate and does not show appreciable changes down to 80 cm^{-1} when varying the gate voltage. Above 1100 cm^{-1} the easily recognizable sharp peaks are due to the first and second order optical phonon Raman processes of the graphene layer. In this work we focus on the low intensity continuum below it.

Figures 1(c) and 1(d) display the evolution of the polarization resolved continuum by varying the gate voltage. While the continuum is essentially independent from the

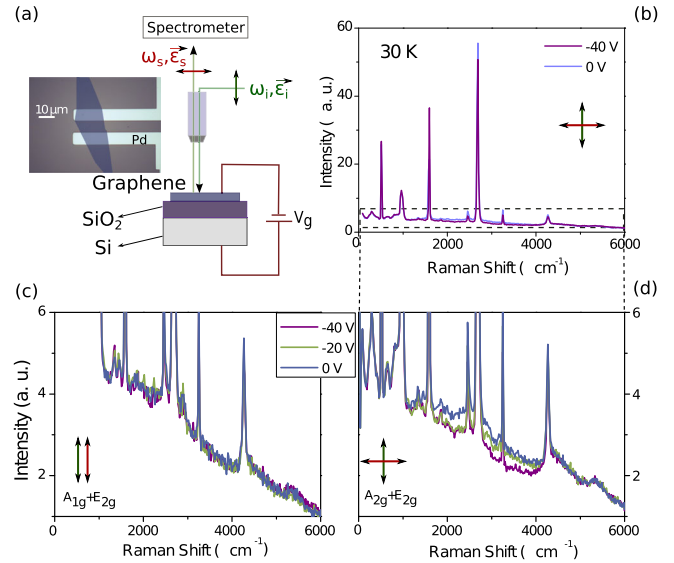


FIG. 1. (a) Optical microscope image and schematic drawing of the device and Raman setup. $\omega_{i,s}$ and $\epsilon_{i,s}$ are the frequency and polarization of the in-coming and scattered photons. The Raman shift is defined as $\omega = \omega_i - \omega_s$. (b) Cross-polarization spectra recorded at two different gate voltages: $V_g = 0$ and $V_g = -40$ V in the $0 - 6000 \text{ cm}^{-1}$ frequency range. The sharp peaks are due to optical phonons (first and higher order process) of Si (below 1100 cm^{-1}) and of graphene (above 1100 cm^{-1}). (c) and (d) Polarization resolved changes in the electronic Raman continuum for parallel polarizations (c) and cross polarizations (d) at three different gate voltages.

gate voltage in parallel polarizations, a clear and reproducible gate-dependent effect is observed for cross polarizations: with increasing gate voltage the continuum shows a suppression of intensity whose onset shifts to higher frequency. The suppression is not complete and concerns at most 20% of the overall continuum intensity in cross polarization. The gate and polarization dependences indicate two distinct contributions to the continuum intensity. One is independent of the gate voltage and dominates the spectra in parallel polarizations configuration. We assign it to residual Raman scattering signal from the Si/SiO₂ substrate and to luminescence coming from residual trapped impurities. Part of it could also be due to Coulomb assisted higher order ERS processes in graphene as discussed in Refs. [38,41]. The second contribution is gate dependent and only observed in a cross-polarizations configuration. Its strong polarization dependence indicates that it is due to ERS by excitations of A_{2g} symmetry originating from the graphene layer. As discussed below, the symmetry assignment is in agreement with the theoretical prediction of Kashuba *et al.* [29,30] for Raman-active electron-hole interband transitions across the Dirac cone involving bands with opposite chiralities.

Proceeding with the analysis of the spectra we note that the above observations suggest the following decomposition for the continuum intensity I :

$$I(\omega, V_g) = \alpha(\omega)[I_0 + I_{\text{ERS}}(\omega, V_g)], \quad (1)$$

where I_{ERS} is the gate-dependent ERS intensity from the graphene layer and I_0 is the gate-independent intensity coming from all other sources of background as discussed above. $\alpha(\omega)$ accounts for the instrumental spectral response which is connected to factors such as the wavelength dependence of the diffraction grating reflectivity and the CCD (charge coupled device) quantum efficiency. It also accounts for wavelength-dependent interference effects due to the presence of the substrate [42]. While all these corrections can, in principle, be estimated and corrected for, we choose a simpler way to extract information on the spectral dependence of I_{ERS} as a function of gate voltage. Indeed, the raw spectra can be normalized with the one taken at the Dirac voltage V_D , $I(V_D)$, defined as the gate voltage at which the Fermi level is at the Dirac (or charge neutrality) point: $E_F(V_g = V_D) = 0$. We can define the ratio R

$$R(\omega, V_g) = \frac{I(\omega, V_g)}{I(\omega, V_D)} = \frac{I_0 + I_{\text{ERS}}(\omega, V_g)}{I_0 + I_{\text{ERS}}(\omega, V_D)}, \quad (2)$$

which is independent from α and thus free from instrumental artifacts. As pristine graphene samples are generally doped by residual impurities and/or contaminants, the Dirac voltage was estimated by following the evolution of the G -band frequency with the gate voltage [18–20], yielding $V_D = 20$ V [43].

For clarity, the optical phonons were first subtracted from the raw spectra, at each gate voltage, using Voigt profiles. This could, however, only be done reliably above 1100 cm^{-1} . Below 1100 cm^{-1} the phonon contributions coming from the Si substrate were found to be too broad and intense to allow for an unambiguous extraction of the small gate-induced changes in the continuum underneath. The resulting phonon-free continua above 1100 cm^{-1} were then divided by the spectrum at the Dirac voltage in order to obtain $R(\omega, V_g)$ which is plotted in Fig. 2(a). As the gate voltage deviates from the Dirac voltage, R is increasingly suppressed and the onset of suppression moves progressively to higher energies, reaching $\sim 4000 \text{ cm}^{-1}$ for $V_g = -40$ V. The behavior of R bears a striking similarity with gate-dependent optical conductivity data performed on similar devices [6,8,10].

We now compare the experimental data with the theoretical expectations of the ERS intensity in graphene. To lowest order, the noninteracting ERS intensity arising from vertical electron-hole interband excitations in graphene reads [29,46,47] [33]

$$I_{\text{ERS}}(\omega) = \gamma^2(\epsilon_i, \epsilon_s)\omega \left[f\left(-\frac{\hbar\omega}{2} - E_F\right) - f\left(\frac{\hbar\omega}{2} - E_F\right) \right], \quad (3)$$

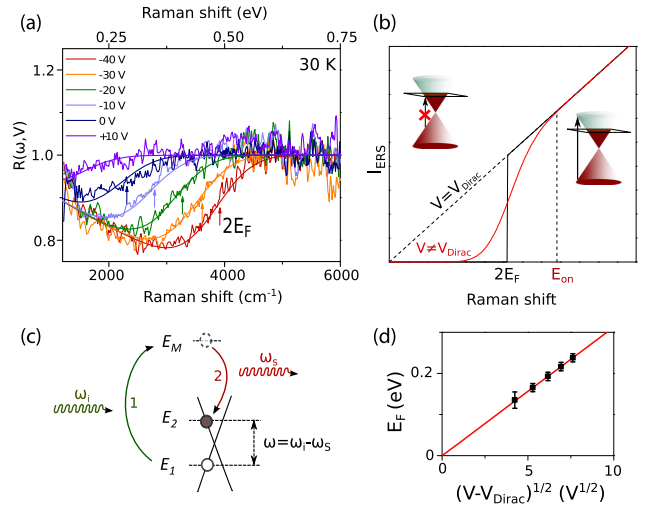


FIG. 2. (a) Experimental and theoretical gate dependence of $R(\omega, V_g)$ at $T = 30$ K (see text) [44]. (b) Evolution of the theoretical I_{ERS} in graphene when the Fermi level is at the Dirac point (dotted straight line), and at finite E_F (solid lines). The solid black curve is for a homogenous sample at $T = 0$ K [Eq. (3)]. The solid red line represents the finite temperature spectrum with a Gaussian distribution of Fermi energy. The insets in (b) show schematics of vertical interband electron-hole excitations which are Pauli blocked for $\omega < 2E_F$. (c) Schematic drawing of the nonresonant ($\omega_i \neq E_M - E_1$) two-step Raman process for interband electron-hole excitations via an intermediate virtual state [33]. E_1 , E_M , and E_2 are the energies of the initial, intermediate, and final electronic states. The ordering of the process is indicated explicitly: the first (second) step involves a photon induced vertical transition from the initial (virtual) state to the virtual (final) electronic state. (d) Fermi energy plotted as a function of the square root of the gate voltage. The red line is the theoretical expectation computed using the estimated gate capacitance of the device. The black dots were extracted from the R data in (a) using the midpoint energy as an estimate of the inflection point [45].

where $f(E) = [1 + e^{(E/k_B T)}]^{-1}$ is the Fermi-Dirac distribution. γ is the Raman vertex that describes the electron-photon interaction process and depends on the in-coming and out-going photon polarizations. In general, both direct contact processes and two-step processes involving a virtual excitation can contribute to ERS intensity [33,35]. As shown by Kashuba *et al.* [29], in the case of graphene and for excitation photon energies in the visible range, nonresonant two-step processes are the dominant ones for interband electron-hole excitations. This is in contrast to conventional two-dimensional electron gas in semiconductor heterostructures, where ERS is generally studied in the resonant regime, with incident photon energies ω_i tuned close to the fundamental gap of the semiconductor [48]. In graphene, the associated nonresonant Raman vertex has A_{2g} symmetry [29]: it is nonzero only for cross linear photon polarizations in agreement with our experimental data. As shown in Fig. 2(b), at the Dirac point the theoretical ERS

intensity has a linear in-frequency spectral dependence, while away from the Dirac point it displays a threshold at $2E_F$ due to Pauli blocking. Except for the linear in-frequency term, the ERS frequency dependence is very similar to the optical conductivity and the approximate relation $I_{\text{ERS}}(\omega) \sim \omega\sigma_1(\omega)$ holds for graphene [47]. As typical graphene samples display inhomogeneous carrier doping, spatial fluctuations of the Fermi energy were also considered and assumed to follow a Gaussian distribution [see Fig. 2(b)].

In order to compare with the experimental data, a theoretical R was calculated by dividing each theoretical spectra by the one at the Dirac voltage. The Fermi energies were chosen assuming the standard relationship between the gate voltage and the density: $n = C(V_g - V_{\text{Dirac}})/e$ with $E_F = -\text{sgn}(n)\hbar v_F \sqrt{(\pi|n|)}$, using the calculated geometrical capacitance of the device ($C = 110 \text{ aF}/\mu\text{m}^2$) and a Fermi velocity $v_F = 10^6 \text{ ms}^{-1}$. The theoretical results are superimposed on the experimental data in Fig. 2(a) for several gate voltages. The agreement between theory and experiment is remarkable given that the only free parameter is the standard deviation of the Gaussian distribution of Fermi energy. In our case $\delta E_F \sim 50 \text{ meV}$ gave the best fits to the data. This value is consistent with previous estimations for supported graphene samples [19,49,50]. We note, however, that other parameters, such as the finite electron lifetimes, can also contribute to the observed broadening of the $2E_F$ threshold. We thus consider this value of δE_F as an upper limit [33]. In Fig. 2(d) we show that the Fermi energy can also be reliably obtained directly from the R data by identifying the inflection point of the spectra [shown with an arrow in Fig. 2(a)] with $2E_F$.

It is illuminating to draw a parallel between the observed gate-dependent ERS continuum and the well-known behavior of the G -band linewidth. Indeed, apart from the Raman vertex prefactor, the frequency dependence of the ERS intensity is essentially given by the imaginary part of the electron polarizability of graphene, $\Pi''(\omega, q=0)$ (see, e.g., Refs. [51,52] and the Supplemental Material). On the other hand, as first noted by Ando [31], and observed experimentally [18–20], due to electron-phonon coupling the G -band linewidth Γ_G contains a contribution, $\Delta\Gamma_G$, which arises from Landau damping by electron-hole excitation processes and is given by the imaginary part of the electron polarizability at the phonon frequency: $\Delta\Gamma_G \sim \Pi''(\omega = \omega_G, q=0)$. The only difference between ERS and G -band renormalization processes is the vertices involved: the Raman vertex γ and the electron-phonon coupling constant g , respectively (see inset in Fig. 3). The gate dependence of the G -band linewidth is thus directly proportional to the intensity of the ERS continuum at the phonon frequency:

$$\Delta\Gamma_G \sim I_{\text{ERS}}(\omega = \omega_G). \quad (4)$$

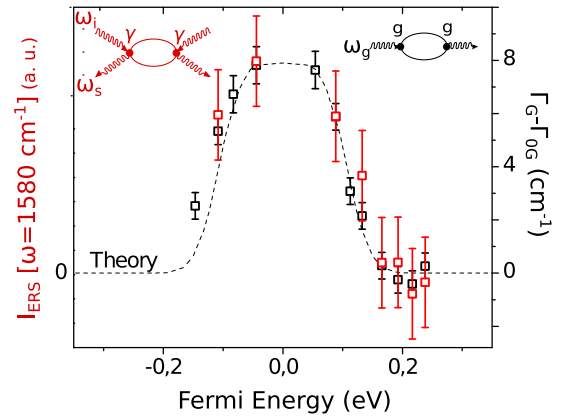


FIG. 3. Evolution of the ERS intensity at 1580 cm^{-1} (red dots) and of the G -band change in linewidth $\Delta\Gamma_G = \Gamma_G - \Gamma_0$ (black dots) as a function of the Fermi energy. Γ_G is the observed linewidth and Γ_0 a gate voltage independent contribution to the linewidth arising from lattice anharmonicity and disorder effects. The dotted line is the theoretical expectation for $I_{\text{ERS}}(1580 \text{ cm}^{-1})$ after a convolution with a Gaussian distribution of Fermi energy with $\delta E_F \sim 50 \text{ meV}$. The insets show Feynman diagrams for the ERS intensity (red) and electron-phonon induced G -band renormalization (black). See Ref. [33] for details about the ERS vertex.

Figure 3 displays the gate voltage dependence of the ERS continuum taken at the G -band frequency $I_{\text{ERS}}(\omega = 1580 \text{ cm}^{-1})$ and the change in linewidth of the G -band $\Delta\Gamma_G$, measured on the same spot but with a higher resolution. The overall agreement between both quantities provides a direct evidence of their common link to the electron polarizability of graphene and gives an unified picture of both effects.

In conclusion, we have observed a gate-dependent ERS signal from a single-layer graphene device. The gate voltage and light polarization dependences of the signal are fully consistent with interband electron-hole excitations created by a nonresonant Raman process. While Raman scattering in carbon-based materials has been traditionally confined to the study of optical phonons, our work demonstrates the ability of Raman scattering in exploring electronic excitations of 2D materials even far away from resonance. It paves the way for promising future studies of interaction induced effects in cleaner devices, which have remained hitherto inaccessible to most spectroscopies.

This work was supported by a C'Nano grant (Optographene) from Ile-de-France region and by a LABEX SEAM (Science and Engineering for Advanced Materials and devices) Grants (No. ANR 11 LABX 086, No. ANR 11 IDEX 05 02). The authors thank Indranil Paul and Dimitri Maslov for fruitful discussions, and the staff of the MPQ laboratory clean room, Stephan Suffit, Christophe Manquest, and Pascal Filloux for their precious technical support.

- *elisa.riccardi@univ-paris-diderot.fr
†yann.gallais@univ-paris-diderot.fr
- [1] K. S. Novoselov, A. K. Geim, S. V. Morosov, D. Jiang, Y. Zhang, S. V. Dubonos, I. V. Grigorieva, and A. A. Firsov, *Science* **306**, 666 (2004).
 - [2] K. S. Novoselov, A. K. Geim, S. V. Morosov, D. Jiang, M. I. Katsnelson, I. V. Grigorieva, S. V. Dubonos, and A. A. Firsov, *Nature (London)* **438**, 197 (2005).
 - [3] Y. Zhang, Y. W. Tan, H. L. Stormer, and P. Kim, *Nature (London)* **438**, 201 (2005).
 - [4] K. F. Mak, L. Ju, F. Wang, and T. F. Heinz, *Solid State Commun.* **152**, 1341 (2012).
 - [5] D. N. Basov, M. M. Fogler, A. Lanzara, F. Wang, and Y. Zhang, *Rev. Mod. Phys.* **86**, 959 (2014).
 - [6] Z. Q. Li, E. A. Henriksen, Z. Jiang, Z. Hao, M. C. Martin, P. Kim, H. L. Stormer, and D. N. Basov, *Nat. Phys.* **4**, 532 (2008).
 - [7] K. F. Mak, M. Y. Sfeir, Y. Wu, C. H. Lui, J. A. Misewich, and T. F. Heinz, *Phys. Rev. Lett.* **101**, 196405 (2008).
 - [8] J. Horng, C.-F. Chen, B. Geng, C. Girit, Y. Zhang, Z. Hao, H. A. Bechtel, M. Martin, A. Zettl, M. F. Crommie *et al.*, *Phys. Rev. B* **83**, 165113 (2011).
 - [9] H. Yan, F. Xia, W. Zhu, M. Freitag, C. Dimitrakopoulos, A. A. Bol, G. Tulevski, and P. Avouris, *ACS Nano* **5**, 9854 (2011).
 - [10] L. Ren, Q. Zhang, J. Yao, Z. Sun, R. Kaneko, Z. Yan, S. Nanot, Z. Jin, I. Kawayama, M. Tonouchi *et al.*, *Nano Lett.* **12**, 3711 (2012).
 - [11] I. Maeng, S. Lim, S. J. Chae, Y. H. Lee, H. Choi, and J.-H. Son, *Nano Lett.* **12**, 551 (2012).
 - [12] F. Wang, Y. Zhang, C. Tian, C. Girit, A. Zettl, M. Crommie, and Y. R. Shen, *Science* **320**, 206 (2008).
 - [13] M. L. Sadowski, G. Martinez, M. Potemski, C. Berger, and W. A. de Heer, *Phys. Rev. Lett.* **97**, 266405 (2006).
 - [14] Z. Jiang, E. A. Henriksen, L. C. Tung, Y. J. Wang, M. E. Schwartz, M. Y. Han, P. Kim, and H. L. Stormer, *Phys. Rev. Lett.* **98**, 197403 (2007).
 - [15] E. A. Henriksen, P. Cadden-Zimansky, Z. Jiang, Z. Q. Li, L. C. Tung, M. E. Schwartz, M. Takita, Y. J. Wang, P. Kim, and H. L. Stormer, *Phys. Rev. Lett.* **104**, 067404 (2010).
 - [16] A. C. Ferrari and D. M. Basko, *Nat. Nanotechnol.* **8**, 235 (2013).
 - [17] L. M. Malard, M. Pimenta, G. Dresselhaus, and M. S. Dresselhaus, *Phys. Rep.* **473**, 51 (2009).
 - [18] A. C. Ferrari, J. C. Meyer, V. Scardaci, C. Casiraghi, M. Lazzeri, F. Mauri, S. Piscanec, D. Jiang, K. S. Novoselov, S. Roth *et al.*, *Phys. Rev. Lett.* **97**, 187401 (2006).
 - [19] J. Yan, Y. Zhang, P. Kim, and A. Pinczuk, *Phys. Rev. Lett.* **98**, 166802 (2007).
 - [20] S. Pisana, M. Lazzeri, C. Casiraghi, K. S. Novoselov, A. K. Geim, A. C. Ferrari, and F. Mauri, *Nat. Mater.* **6**, 198 (2007).
 - [21] C. Faugeras, M. Amado, P. Kossacki, M. Orlita, M. Sprinkle, C. Berger, W. A. de Heer, and M. Potemski, *Phys. Rev. Lett.* **103**, 186803 (2009).
 - [22] J. Yan, S. Goler, T. D. Rhone, M. Han, R. He, P. Kim, V. Pellegrini, and A. Pinczuk, *Phys. Rev. Lett.* **105**, 227401 (2010).
 - [23] S. Remi, B. B. Goldberg, and A. K. Swan, *Phys. Rev. Lett.* **112**, 056803 (2014).
 - [24] C. Faugeras, M. Amado, P. Kossacki, M. Orlita, M. Kuhne, A. A. L. Nicolet, Y. I. Latyshev, and M. Potemski, *Phys. Rev. Lett.* **107**, 036807 (2011).
 - [25] S. Berciaud, M. Potemski, and C. Faugeras, *Nano Lett.* **14**, 4548 (2014).
 - [26] C. Faugeras, S. Berciaud, P. Leszczynski, Y. Henni, K. Nogajewski, M. Orlita, T. Taniguchi, K. Watanabe, C. Forsythe, P. Kim *et al.*, *Phys. Rev. Lett.* **114**, 126804 (2015).
 - [27] Y. S. Ponomov, A. V. Ushakov, and S. V. Streltsov, *Phys. Rev. B* **91**, 195435 (2015).
 - [28] H. Farhat, S. Berciaud, M. Kalbac, R. Saito, T. F. Heinz, M. S. Dresselhaus, and J. Kong, *Phys. Rev. Lett.* **107**, 157401 (2011).
 - [29] O. Kashuba and V. I. Fal'ko, *Phys. Rev. B* **80**, 241404 (2009).
 - [30] O. Kashuba and V. I. Fal'ko, *New J. Phys.* **14**, 105016 (2012).
 - [31] T. Ando, *J. Phys. Soc. Jpn.* **75**, 124701 (2006).
 - [32] C. R. Dean, A. F. Young, I. Meric, C. Lee, L. Wang, S. Sorgenfrei, K. Watanabe, T. Taniguchi, P. Kim, K. L. Shepard *et al.*, *Nat. Nanotechnol.* **5**, 722 (2010).
 - [33] See Supplemental Material at <http://link.aps.org/supplemental/10.1103/PhysRevLett.116.066805>, which includes Refs [5,8,29,34–40] for details on the Raman selection rules, ERS processes, and calculations of the ERS response in graphene including finite lifetime and temperature effects.
 - [34] W. Hayes and R. Loudon, *Scattering of Light by Crystals* (Dover, New York, 2004).
 - [35] P. A. Wolff, *Phys. Rev. Lett.* **16**, 225 (1966).
 - [36] T. P. Devereaux and R. Hackl, *Rev. Mod. Phys.* **79**, 175 (2007).
 - [37] N. Ashcroft and D. Mermin, *Solid State Physics* (Holt-Saunders, New York, 1976).
 - [38] E. H. Hasdeo, A. R. T. Nugraha, M. S. Dresselhaus, and R. Saito, *Phys. Rev. B* **90**, 245140 (2014).
 - [39] P. M. Platzman, *Phys. Rev.* **139**, A379 (1965).
 - [40] A. Zawadowski and M. Cardona, *Phys. Rev. B* **42**, 10732 (1990).
 - [41] E. H. Hasdeo, A. R. T. Nugraha, K. Sato, M. S. Dresselhaus, and R. Saito, *Phys. Rev. B* **88**, 115107 (2013).
 - [42] D. Yoon, H. Moon, Y. W. Son, J. S. Choi, B. H. Park, Y. H. Cha, Y. D. Kim, and H. Cheong, *Phys. Rev. B* **80**, 125422 (2009).
 - [43] See Supplemental Material at <http://link.aps.org/supplemental/10.1103/PhysRevLett.116.066805>, which includes Refs [19, 20, 31] for the analysis of gate-dependent G-band data on this device.
 - [44] See Supplemental Material at <http://link.aps.org/supplemental/10.1103/PhysRevLett.116.066805> for additional ERS data on a second device at room temperature.
 - [45] See Supplemental Material at <http://link.aps.org/supplemental/10.1103/PhysRevLett.116.066805> for details on the determination of $2E_F$ using $R(\omega)$ data.
 - [46] H. Y. Lu and Q. H. Wang, *Chin. Phys. Lett.* **25**, 3746 (2008).
 - [47] A. G. Grushin, B. Valenzuela, and M. A. H. Vozmediano, *Phys. Rev. B* **80**, 155417 (2009).
 - [48] A. Pinczuk and G. Abstreiter, *Light Scattering in Solids V* (Springer, New York, 1989), Vol. 66.
 - [49] J. Martin, N. Akerman, G. Ulbricht, T. Lohman, J. H. Smet, K. von Klitzing, and A. Yacobi, *Nat. Phys.* **4**, 144 (2008).
 - [50] G. Froehlicher and S. Berciaud, *Phys. Rev. B* **91**, 205413 (2015).
 - [51] B. Wunsch, T. Stauber, F. Sols, and F. Guinea, *New J. Phys.* **8**, 318 (2006).
 - [52] E. H. Hwang and S. Das Sarma, *Phys. Rev. B* **75**, 205418 (2007).